Dynamic Multi-Objective Optimization Applied to a Solar-Geothermal Multi-Generation System for Hydrogen Production, Desalination, and Energy Storage

Ali Sohani [a], Fatemeh Delfani [b], Mohammadmehdi Hosseini [a], Hoseyn Sayyaadi [a], Nader Karimi [c,d], Larry K.B. Li [e], Mohammad Hossein Doranehgard [e,f,1]

[a] Lab of Optimization of Thermal Systems' Installations, Faculty of Mechanical Engineering-Energy Division, K.N. Toosi University of Technology, P.O. Box: 19395-1999, No. 15-19, Pardis St., Mollasadra Ave., Vanak Sq., Tehran 1999 143344, Iran

[b] Department of Mechanical Engineering, Semnan Branch, Islamic Azad University, Semnan, Iran

[c] School of Engineering and Materials Science, Queen Mary University of London, London E1 4NS, United Kingdom

[d] James Watt School of Engineering, University of Glasgow, Glasgow G12 8QQ, United Kingdom

[e] Department of Mechanical and Aerospace Engineering, Hong Kong University of Science and Technology, Clear Water Bay, Hong Kong

[f] Department of Civil and Environmental Engineering, School of Mining and Petroleum Engineering, University of Alberta, Edmonton, Alberta T6G 1H9, Canada

Abstract

The design of optimal energy systems is vital to achieving global environmental and economic targets. In the design of solar-geothermal multi-generation systems, most previous investigations have relied on the static multi-objective optimization approach (SMOA), which may leave considerable room for improvement under certain conditions. In this numerical study, the optimal condition at which to operate a solar-geothermal multi-generation system – which

[1] Corresponding author; Email address: doranehg@ualberta.ca (M.H. Doranehgard).

can simultaneously produce hydrogen, fresh water, electricity, and heat, along with storing energy − is determined via a dynamic multi-objective optimization approach (DMOA). Optimization is performed using a combination of NSGA-II and TOPSIS, and the results are benchmarked against those of SMOA. The decision variables include the solar area, geothermal water extraction mass flow, and hydrogen storage pressure. The objective functions include the production of electricity, heat, hydrogen, and fresh water, along with the exergy and energy efficiencies and the payback period. It is found that when compared with SMOA, DMOA can significantly improve all the objective functions. The annual production of electricity, heat, hydrogen, and fresh water increases by 14.4, 16.1, 13.5, and 14.3%, respectively, while the average annual exergy and energy efficiencies increase by 5.2 and 3.0%, respectively. The use of DMOA also reduces the payback period from 5.56 to 4.43 years, with a 4.4% reduction in hydrogen storage pressure. This shows that compared with a static approach such as SMOA, DMOA can improve the exergy and energy efficiencies, economic viability, and safety of a solar-geothermal multi-generation system.

Keywords: *Multi-effect desalination technology; Dynamic multi-objective optimization; Solar geothermal energies combination; Techno-economic analysis; Hydrogen production.*

Nomenclature

Symbols

d	Distance parameter in TOPSIS method
OBF	Objective function
obf	Dimensionless objective function
min	Minimize
max	Maximize
CLI	Closeness index
N	Number of time intervals
no	Number of objectives
X	Decision variable
t	Time

Greek symbols

Δ	Difference

Subscripts

i	Counter for decision variable number
ideal	Ideal
k	Counter for the time interval in DMOA
non-ideal	Non-ideal

Abbreviations

TOPSIS	Technique for order of preference by similarity to ideal solution
PSO	Particle swarm optimization
SMOA	Static multi-objective optimization approach
PV	Photovoltaic
NSGA-II	Non-dominated sorting GA II

GWO	Grey wolf optimizer
PEM	Proton exchange membrane
GA	Genetic algorithm
TEG	Thermoelectric generator
PTSC	Parabolic trough solar collector
SOFC	Solid Oxide Fuel Cell
ANN	Artificial neural network
CCHP	Combined cooling, heating, and power
ORC	Organic Rankine cycle
STPV	Solar thermal photovoltaic
RSM	Response surface methodology
DMOA	Dynamic multi-objective optimization approach
EL	electrolyzer

1. Introduction

The growth in the number of people living on Earth, along with problems arising from energy security and climate change, has highlighted the need to deploy energy systems that are more efficient and economical [1]. Among the different sources of energy available, renewable sources, such as solar and geothermal, hold particular promise [2]. The conversion and storage of renewable energy via hydrogen is gaining traction in various fields [3]. When compounded with water scarcity problems, this has led to the development of multi-generation systems that can simultaneously produce electricity, heat, hydrogen, and fresh water [4]. It is therefore unsurprising that significant research has been done to analyze and optimize such multi-generation systems [5].

Temiz et al. [1] conducted a thermodynamical study, based on energy and exergy analysis, of a system integrating solar and thermal energy to produce fresh water, hydrogen, electricity, and space heating. The system was located in California. It was observed that the highest energy efficiency (27.56%) occurs in November, but that the highest exergy efficiency (17.3%) occurs in January. The system produced 296.9 tons of hydrogen.

Abdelshafy et al. [6] proposed an optimization method based on PSO–GWO (Particle Swarm Optimization – Grey Wolf Optimizer) to optimize the size of the components of a grid-connected

reverse-osmosis desalination plant integrated with a hybrid energy system, and to decrease its cost. It was found that PSO-GWO can offer superior optimization performance when compared with each method applied separately. Adding a diesel generator in the hybrid system was found to reduce costs significantly.

Sayyaadi et al. [7] presented a conceptual design for a thermochemical Cu-Cl cycle with a capacity of 6000 kg per day. Through pinch analysis, the efficiency of the cycle could be increased by 10.2%. Further optimization was conducted in which the objective functions included the cost of hydrogen, energy efficiency and exergy efficiency. By choosing three design variables and with the help of TOPSIS, the researchers achieved thermal and exergy efficiencies of 49.83% and 58.23%, respectively, at a cost of $6.33 per kilogram for hydrogen.

Habibollahzade et al. [8] investigated a system featuring a thermoelectric generator (TEG), a parabolic trough solar collector (PTSC), and a PEM (proton exchange membrane) in terms of exergy and exergoeconomic performance using a genetic algorithm. The results showed that the use of TEG, instead of a condenser, not only improves exergy efficiency but also reduces the total unit cost. The optimized state of the system had the exergy efficiency of 12.8 percent.

Integrating PVT panels and PEME with a Solid Oxide Fuel Cell (SOFC) system, Cao et al. [9] attempted to produce primary fuel that is rich in hydrogen. A tri-objective optimization based on exergy, economics, and environmental performance was performed to assess the proposed system relative to the conventional system. It was observed that the output power and CO_2 emissions of the model were 8.7% and 12.9% higher than that of a conventional system, respectively.

Using RSM and ANN-GA, Yahya et al. [10] optimized the catalytic steam reformation of toluene used for hydrogen production. The temperature, feed flow rate, catalyst weight and molar ratio of

steam to carbon were considered the optimization variables. The results show that ANN-GA, which had a higher R^2 value (coefficient of determination) and lower RSME value (root mean square error), can raise the process efficiency to 92.6%, significantly above what RSM can achieve.

Gutierrez-Martin et al. [11] modeled a system in which a photovoltaic cell was integrated with an electrolyzer (EL) so as to evaluate its capacity, component operation, and costs. Their study was conducted in two cities (Madrid and Fisciano), and considered the system with and without batteries. The results showed that despite increasing the costs and energy loss, the use of batteries can reduce the electrolyzer size. Moreover, it was concluded that operating electrolyzer at a fixed rate requires larger batteries and PV cells.

Behzadi et al. [12] proposed a new model based on solar energy with the integration of a TEG for hydrogen production and cooling. The aim was to compare this system, in terms of energy, exergy, and exergoeconomic performance, with a conventional cogeneration unit in which a condenser is used instead of TEG. The results showed that the integration of TEG improved exergy efficiency, hydrogen production and total cost.

Keshavarzzadeh et al. [13] analyzed a CCHP system consisting of a TES, PTSCs, a PEMFC, an ORC, a PEME, and a Li-Br chiller. Results showed that when TES and PEMFC are used together, the output power can increase by 3% during the day and by 10% during the night. Then, a NSGA-II method, with cost and exergy efficiency as the objective functions, was used to optimize the system state, achieving 80% and 0.06 dollar per second as the optimum values. With optimization with one objective, the analogous results were 57% and 0.044 dollar per second.

Daneshpour and Mehrpooya [14] proposed a new model of a system consisting of a photovoltaic device and solid oxide electrolyzer cell whose main product was hydrogen but which produced

oxygen as a byproduct. A series of STPV devices were used to supply the required power for the steam electrolyzer. The results showed that STPVs can potentially be used to convert solar energy to supply electrolyzers working under high temperatures.

Saleem et al. [15] designed an annual simulation of a system used for solar heating of water for different climate conditions in Karachi, Pakistan. The main objective was to use TRNSYS to identify the refrigerant most capable of exchanging heat. The results indicated that the key factor is the thermal conductivity of the refrigerant. Ammonia was found to be the best refrigerant, with energy gains of 8900 and 7500 kJ per hour for July and January.

Izadi et al. [16] sought to improve the performance of a power plant featuring a gas turbine, which consists of thermoelectric generators, a single flash desalinated unit, and a single effect Li-Br chiller. Results indicated that the inlet air preheating could be effective in reducing CO and CO_2 emissions, but at the expense of increasing NO emissions. Furthermore, with the application of multi-objective optimization, it was found that the use of solar energy decreased fuel consumption by 0.1871 $kg.s^{-1}$ and increased the exergy efficiency by 2.92%.

Aided by multi-objective optimization, Tebibel et al. [17] proposed a new methodology to improve the design of a wind energy driven H_2 production system and to reduce its environmental effects and production costs. The results showed that the optimum design can be effective in reducing both technical and economic objectives. Under the experimental conditions examined, the simulation showed a levelized H_2 cost which is equal to 33.70 dollar per kg, and energy dump possibility of 10%.

Taking an economics viewpoint, Koleva et al. [18] used simulations of a PV-EL system to increase its NPW (net present worth). They considered different financial methods and weather conditions

in California. The results showed that a system with market settings similar to combined retail and wholesale could offer a range of potentially cost-competitive solutions, leading to a hydrogen production cost between $6.2 per kg and $6.6 per kg.

Alirahmi et al. [19] performed an exergoeconomic and exergy evaluation of a system that produced electricity, fresh water, and hydrogen for three different solar radiations (high, low and no radiation). They then performed optimization based on a genetic algorithm. It was found that the cost per unit of the system's exergy has a direct correlation with the current density and an inverse correlation with the electrolyzer temperature as well as the peak temperature of the desalination unit. The exergy efficiencies ranged from 2.52% to 5.39%.

Farsi et al. [20] investigated a Cu-Cl cycle in Aspen Plus to optimize the exergy efficiency and costs of hydrogen generation using a genetic algorithm integrated with artificial intelligence. For different operating conditions, they also conducted a sensitivity analysis for the studied model. Siddiqui and Dincer [21] presented a new model for a solar-geothermal system featuring multi-generation capabilities including those for fresh water, cooling, hydrogen and electricity; these researchers evaluated the thermodynamics of the model and found energy and exergy efficiencies of 42.3% and 21.3%, respectively. Yuksel et al. [22] presented a new multi-generation system in which a Brayton cycle functioned as the main unit using methane gas and was integrated with an organic Rankine cycle to produce hydrogen, electricity, ammonia, drying, freshwater, cooling, and heating. After a thermodynamic analysis, the energy and exergy efficiencies of the entire system were calculated to be 69.09% and 65.42%, respectively. Ishaq and Dincer [23] conducted a comprehensive dynamic analysis of a solar-driven system, which was used for electricity production and ammonia synthesis. The system also utilized a PEM electrolyzer for hydrogen generation, and its performance was evaluated under different radiation intensities. The greatest

production of hydrogen and ammonia was 5.85 and 1.38 $mol.s^{-1,}$ respectively, which occurred in the month of June.

When photovoltaic panels are applied, some materials, including nanofluids, could be utilized for performance enhancement. For instance, Sangeetha et al. [24] conducted experiments to investigate the impact of nanofluids on a photovoltaic-thermal-solar system in which three different nanofluids were chosen as the coolant for the photovoltaic panel. The results showed that the adoption of each of the three nanofluids resulted in increases in electrical power and efficiency. On a similar note, Manigandan et al. [25] considered two different types of water-based nanofluids, based on ZnO and CuO, in order to experimentally examine their influence as coolants in five different photovoltaic fluid collector systems. These researchers reported that the energy efficiency of the system would rise as a result of the use of nanofluid.

A literature review has revealed that despite significant research contributions to date, multi-objective optimization has been applied only conventionally, in the form of a static multi-objective optimization approach (SMOA). As noted previously (e.g. in Ref. [26]), the use of SMOA may leave some optimization potential unrealized under certain conditions. The dynamic multi-objective optimization approach (DMOA), in which changes in the effective system parameters are accounted for throughout the year, has yet to be comprehensively studied. Based on this research gap and the success of DMOA in other energy systems (e.g. evaporative coolers [27]), the present study uses DMOA to optimize a solar-geothermal multi-generation system for simultaneous production of electricity, heat, hydrogen, and fresh water. The results are then benchmarked against those of SMOA in terms of exergy and energy efficiencies, economic viability, and safety. A techno-economic multi-objective optimization is carried out by considering the annual production of electricity, heat, hydrogen, and fresh water, along with the exergy and

energy efficiencies, payback period, and hydrogen storage pressure. The results show that for the specific system under study, DMOA can lead to better performance than SMOA, highlighting the need to adopt a dynamic approach when optimizing solar-geothermal systems.

The aim of this research is to determine the optimal operating conditions of a solar-geothermal multi-generation system via DMOA, where the objective functions include the generation of electricity, heating, hydrogen, and fresh water, as well as the exergy and energy efficiencies and the payback period.

2. Methodology

The details about the methodology are given here. It includes system description and optimization procedure. They are presented in sections 2.1 and 2.2, respectively.

2.1. System description

The investigated system is schematically shown in Figure 1. This system is a multi-generation unit relying on renewable energy. It has many subsystems such as a concentrated solar power system (CSP), a parabolic trough collector (PTC), an energy storage system, a Cu-Cl thermochemical unit for hydrogen production, a multi-effect distillation (MED) unit, a heat pump for building heating, and a trilateral ammonia Rankine cycle for the geothermal system. Saline water enters the system from a water source containing salt, e.g., the ocean. The energy needed to run the system is then extracted by the system itself via devices such as PTC, CSP, and heat exchangers.

As Figure 1 shows, the geothermal water enters the system and undergoes a trilateral ammonia Rankine cycle to supply the required heat. This cycle is responsible for electricity generation. The excess heat from NH_3 is then transferred to a R-134a heat pump via a heat exchanger. From the

separator, steam enters the desalination unit, producing fresh water. The energy for running the Cu-Cl cycle is supplied from TES and CSP. In the first stage of the Cu-Cl cycle, which involves hydrolysis, the reaction of $CuCl_2$ and steam results in the production of HCl and Cu_2OCl_2. In the second step, which involves thermolysis, O_2 and CuCl are produced from the decomposition of Cu_2OCl_2. In the third step, which occurs in the electrolyzer, the reaction of CuCl with HCl results in the production of gaseous hydrogen and aqueous $CuCl_2$. Hydrogen is transferred to the compressor to be stored as compressed fuel, while $CuCl_2$ is transferred to the dryer to be prepared for reuse in the first stage of the Cu-Cl cycle. The Cu-Cl cycle is one of the most common means of H_2 production [28].

Further details on this multi-generation system can be found in the study by Temiz and Dincer [1], in which it was originally introduced.

Tehran, the capital and largest city of Iran, is chosen as the location of this case study. With a population of over 10 million, Tehran is a mega-city that faces severe water scarcity and air pollution. Therefore, the investigated system could be part of a viable solution. It is worth noting that this city has a strong geothermal energy potential, especially in the north-eastern regions [29]. The climatic data for Tehran are extracted from Ref. [30] at a temporal resolution of 10 minutes.

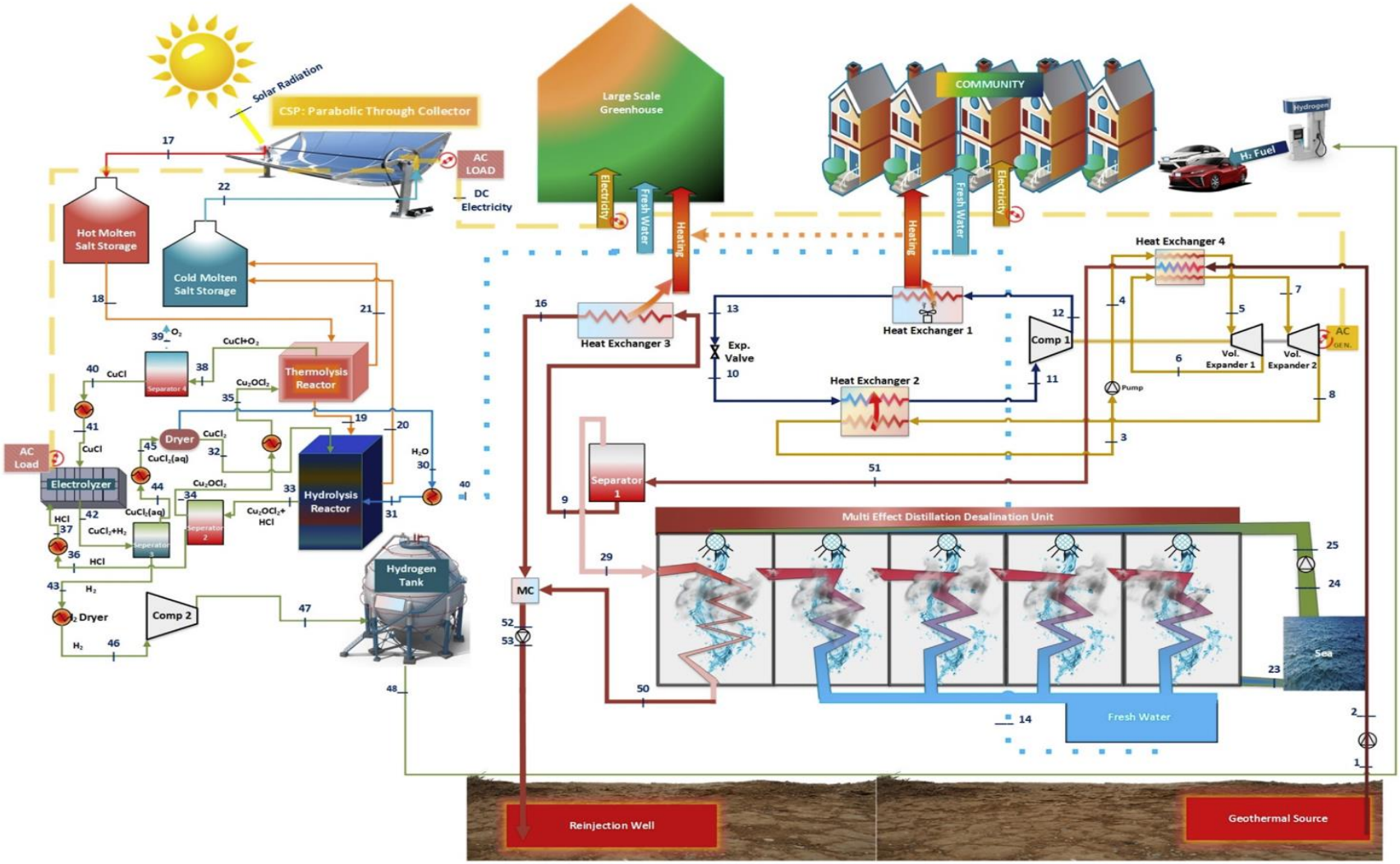

Figure 1. Schematic of the investigated system, as per Ref. [1].

2.2. Optimization procedure

Two different types of optimization methods are used and compared. The first is the static multi-objective optimization approach (SMOA), which is the conventional approach for optimization. The second is the dynamic multi-objective optimization approach (DMOA), which is a novel technique for this specific system. Initially, the list of decision variables and objective functions is provided. Then, the working principles of SMOA and DMOA are explained. After that, information about the case study is presented. Given that both SMOA and DMOA rely on a combination of NSGA-II and TOPSIS, these two methods are also introduced.

Operation of NSGA-II is based on an evolutionary process, which means that the algorithm has to run several times in order to identify the globally optimal point.

The annual production of electricity, heat, H_2, and fresh water in the system, along with the average annual exergy and energy efficiencies, are selected as the objective functions for both SMOA and DMOA; these functions should be maximized. The payback period is also chosen as an objective function, representing the economics, which should be minimized. Therefore, the multi-objective optimization problem takes the form:

$$\begin{cases} \max & \textit{Annual electricity production} \\ \max & \textit{Annual heat production} \\ \max & \textit{Annual } H_2 \textit{ production} \\ \max & \textit{Annual fresh water production} \\ \max & \textit{Annual Average energy efficiency} \\ \max & \textit{Annual Average exergy efficiency} \\ \min & \textit{Payback period} \end{cases} \quad (1)$$

It should be noted that all the considered values of parameters for the cycle and simulation processes are similar to those used in Ref. [1]. Consequently, these values are not repeated here.

The area of the collectors, called the solar area, in addition to the extracted mass flow rate of geothermal water and the H_2 storage pressure, are selected as the decision variables. The lower and upper bounds for the three decision variables are shown in Table 1.

Table (1): Lower and upper bounds for the three decision variables.

Decision variable	Lower bound	Upper bound	Unit
Solar area	0	100,000	m^2
Extracted mass flow rate of geothermal water	0	5,000	$kg.s^{-1}$
H_2 storage pressure	100	500	bar

In order to make the optimization process more practical, it is necessary to use just a few decision variables, and for that reason number of selected decision variables is three. The three chosen variables, including solar area, geothermal water extraction mass flow rate, and hydrogen storage pressure, are reasonably effective for reaching the appropriate optimal condition of the system.

SMOA and DMOA are two viable optimization approaches. In SMOA, the optimization algorithm runs only a single time, and the optimum values of the decision variables and thus the objective functions are determined [31].

In DMOA, the optimization algorithm runs every time interval. Therefore, if there are N time intervals, each with a period of Δt, then the optimization algorithm runs N times. If the value of the ith decision variable from running the optimization algorithm at the k^{th} time interval is $X_{i,j}$, then the value provided by DMOA would be [32]:

$$X_{i,DMOA} = \frac{\sum_{k=1}^{N}\left(X_{i,k,DMOA}\Delta t\right)}{\sum_{k=1}^{N}\left(\Delta t\right)} \quad (2)$$

We use a combination of NSGA-II and TOPSIS. The former is used to find the Pareto optimal frontier (POF), while the latter is used to find the best solution on the POF.

In NSGA-II, an initial population is generated randomly. A comparison is then made between each solution and its counterpart, in order to determine how many solutions dominate the answer. As a hypothetical example, suppose that the objective is to minimize all the objectives, answer Z_2 dominates Z_1 in case the whole elements of Z_2 are not greater than or equal to those of Z_1. The dominancy degree of a solution is the number of points on the POF that dominate it. The answers are then sorted based on their dominancy degrees. According to the algorithm, based on a given ratio, a certain number of solutions remains to create the subsequent population, and the remainder is put aside. In cases where number of points needed to produce the subsequent population is smaller than the number of existing ones, all of them will be chosen, and then, the next population group with a greater dominancy degree will be taken into account. Otherwise, the points which have the identical dominancy degree are sorted based on the crowding distance. The answers that have higher crowding distances will be selected up to the time the required points for generating the subsequent generation are completely gathered. When the algorithm is programmed in this way, the stopping criterion must be checked. If just one of them is met, the algorithm will stop, and non-dominant solutions will form the POF. Otherwise, the algorithm continues.

The TOPSIS decision making method is used to identify the optimal answer among the points on the POF. In TOPSIS, answers are first made dimensionless [32]:

$$obf_{jk} = \frac{OBF_{jk}}{\sqrt{\sum_{j=1}^{no_j}\left[\left(OBF_{jk}\right)^2\right]}} \tag{3}$$

where *obf* and *OBF* refer to the objective function and the dimensionless objective function, respectively. Then, the distances from the ideal and non-ideal answers are determined [32]:

$$d_{ideal,j} = \sqrt{\sum_{k=1}^{no_{obj}} \left(obf_{jk} - obf_{ideal,k} \right)^2} \quad (4)$$

$$d_{non-ideal,j} = \sqrt{\sum_{k=1}^{no_{obj}} \left(obf_{jk} - obf_{non-ideal,k} \right)^2} \quad (5)$$

where d_{ideal} is the distance from the ideal answer and $d_{non\text{-}ideal}$ is the distance from the non-ideal answer. It should be noted that ideal and non-ideal answers are the imaginary solutions that have the best and worst values of the objective functions, respectively.

Ultimately, the closeness index for each solution is determined [32]:

$$CLI_j = \frac{d_{ideal,j}}{d_{ideal,j} + d_{non-ideal,j}} \quad (6)$$

In Eq. (6), CLI is the closeness index. The answer with the smallest value of the closeness index corresponds to the TOPSIS selection.

3. Results and discussion

This section begins with a validation of the simulation framework, and then moves on to present the results of DMOA. These results are compared with those of SMOA for benchmarking.

3.1. Validation

To validate the proposed methodology, the results from Ref. [1] are used. Figure 2 shows good agreement between our data and the data from Ref. [1]. It is worth mentioning that the data in Ref. [1] are for Geysers, California (USA). The maximum and mean error values are 1.7 and 1.2%, respectively, demonstrating the reliability of the framework.

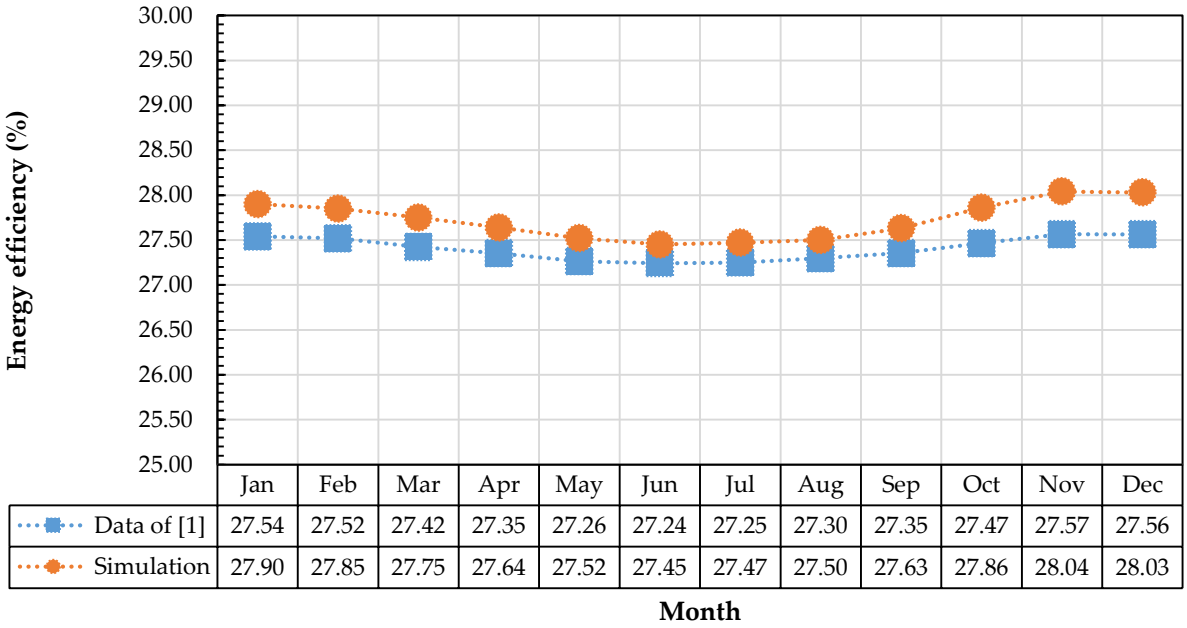

	Jan	Feb	Mar	Apr	May	Jun	Jul	Aug	Sep	Oct	Nov	Dec
Data of [1]	27.54	27.52	27.42	27.35	27.26	27.24	27.25	27.30	27.35	27.47	27.57	27.56
Simulation	27.90	27.85	27.75	27.64	27.52	27.45	27.47	27.50	27.63	27.86	28.04	28.03

Figure 2. Validation of the simulation framework against Ref. [1].

Despite the use of analytical models, there might be errors in the results relative to the actual measurements. One source of error could be phenomena not considered in the modeling. For instance, there could be hotspots on the surface of the PV panel that are not considered in the simulation. In addition, there are measurement errors in recording the experimental meteorological data. However, the low error level in the validation case shows that the modeling approach deployed here is sufficiently reliable for the present study.

3.2. Decision variables

The values of the decision variables for SMOA and DMOA are shown in Table (2). It is found that DMOA tends to utilize a larger solar area and a higher extracted mass flow rate of geothermal water. The values of the first two decision variables are 12.8 and 11.8% higher for DMOA than for SMOA, respectively. However, the H_2 storage pressure tends to decrease from 367.6 bar for SMOA to 351.4 bar for DMOA, a 4.4% reduction. The lower H_2 storage pressure implies a slightly safer system.

Table (2): Values of the decision variables at the optimal condition for SMOA and DMOA.

Decision variable	SMOA	DMOA	Unit
Solar area	20992.7	23688.4	m^2
Extracted mass flow rate of geothermal water	10.832	12.113	$kg.s^{-1}$
H_2 storage pressure	367.6	351.4	bar

3.3. Dynamic multi-objective optimization

The monthly and annual profiles of the technical objective functions are compared between SMOA and DMOA. Later, the payback periods are also compared.

3.3.1. H_2 production

The more solar radiation the system receives, the more H_2 it can produce. Therefore, in the hotter months of the year, more H_2 is produced, regardless of whether DMOA or SMOA is used. Figure 3 shows the monthly variation of H_2 production. It is found that for all months of the year, DMOA produces more H_2 than SMOA. This difference is greatest near summer because, with DMOA, the collector area can be increased such that more solar energy is received and converted. In January, there is a 378.1 kg difference between DMOA and SMOA, with the former and latter producing 10217.3 and 9839.2 kg of H_2, respectively. Moreover, in March, May, and July, DMOA produces 17419.7, 25459.5, and 31827.7 kg of H_2, but the corresponding values for SMOA are 16249.3, 22251.5, and 26557.2 kg. Therefore, DMOA gives 1170.3, 3208.0, and 5270.5 kg more H_2 than SMOA; these numbers are 3.1, 8.5, and 13.9 times those in January, respectively. Figure 3 also shows that July is the month with the highest received solar radiation, the highest H_2 production, and hence the greatest improvement over SMOA. In every month of the year, H_2 production with DMOA is higher than that with SMOA, leading to a higher annual H_2 production as well. Specifically, SMOA leads to 230178.6 kg of H_2 production, whereas DMOA leads to 261251.2 kg, an increase of 13.5%.

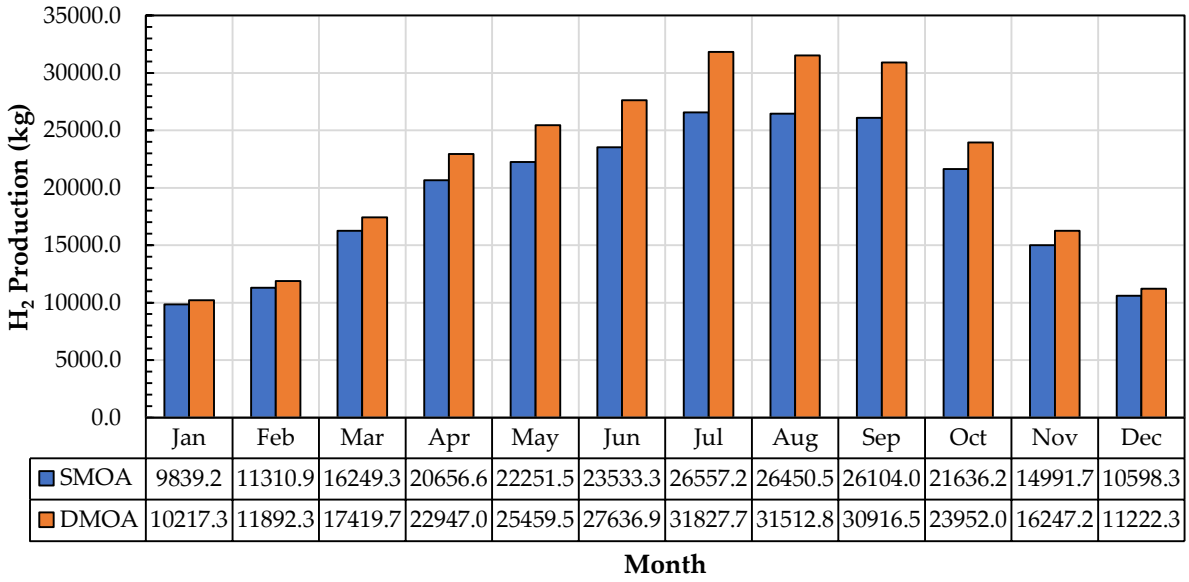

	Jan	Feb	Mar	Apr	May	Jun	Jul	Aug	Sep	Oct	Nov	Dec
SMOA	9839.2	11310.9	16249.3	20656.6	22251.5	23533.3	26557.2	26450.5	26104.0	21636.2	14991.7	10598.3
DMOA	10217.3	11892.3	17419.7	22947.0	25459.5	27636.9	31827.7	31512.8	30916.5	23952.0	16247.2	11222.3

Figure 3. Comparison of monthly H_2 production with DMOA and SMOA.

3.3.2. Fresh water production

Receiving more solar radiation from the sun leads to more input energy for water desalination. Therefore, the same seasonal variations seen in H_2 production are also seen for fresh water production. It is observed that DMOA can increase fresh water production. As Figure 4 shows, fresh water production for February, April, and June rises from 5913.4, 10830.4, and 12295.9 ton with SMOA to 6205.9, 11974.9, and 14422.3 ton with DMOA, respectively. This is equivalent to increases of 4.9, 10.6, and 17.3%, respectively.

Like H_2 production, fresh water production peaks in July, when the irradiance level is at a maximum. During this month, compared with SMOA, DMOA increases fresh water production from 13921.2 to 16934.4 ton, which is a 21.6% improvement. Regarding the annual fresh water production, DMOA gives an increase from 119309.4 to 136333.3 ton, an improvement of 13.5%.

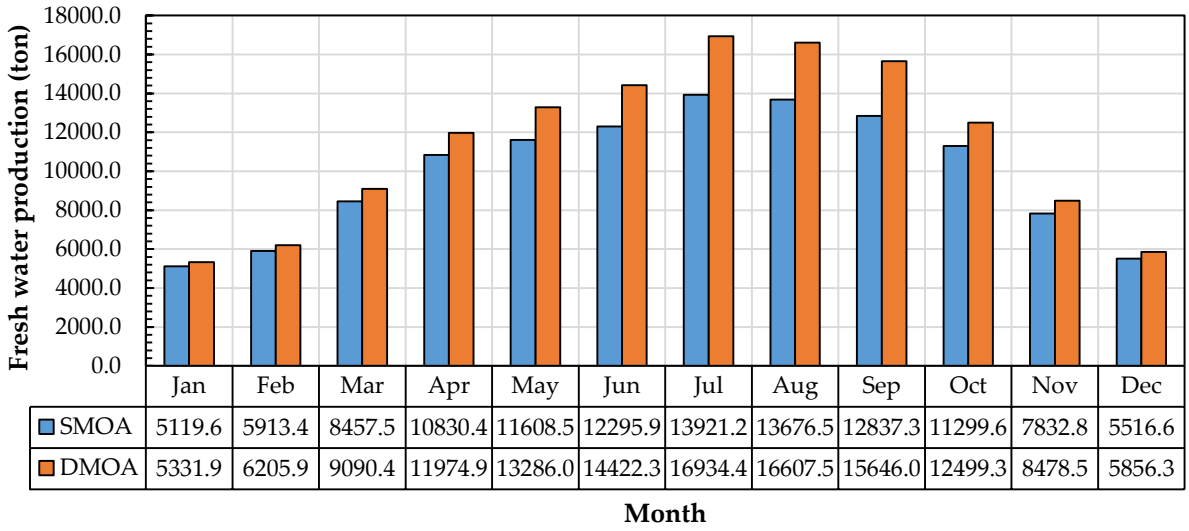

	Jan	Feb	Mar	Apr	May	Jun	Jul	Aug	Sep	Oct	Nov	Dec
SMOA	5119.6	5913.4	8457.5	10830.4	11608.5	12295.9	13921.2	13676.5	12837.3	11299.6	7832.8	5516.6
DMOA	5331.9	6205.9	9090.4	11974.9	13286.0	14422.3	16934.4	16607.5	15646.0	12499.3	8478.5	5856.3

Figure 4. Comparison of monthly fresh water production with DMOA and SMOA.

3.3.3. Energy efficiency

The monthly variation of energy efficiency is shown in Figure 5. It is observed that the energy efficiency dips during the hot months of the year. This is because the energy efficiency is normalized by the received solar radiation, but owing to system inefficiencies, the nominator of this parameter is proportional to an irradiance power below unity. Figure 5 shows that there is a significant improvement in energy efficiency when DMOA is used instead of SMOA. The improvement is weak during the winter but strong during the summer. For instance, in December, October, and August, SMOA gives an energy efficiency of 30.42, 29.66, and 28.56%. The corresponding values for DMOA are 31.09, 30.55, and 29.70%, implying an improvement of 2.2, 3.0, and 4.0%, respectively. Again, July is the month with the greatest improvement in energy efficiency (4.1%). When SMOA is replaced with DMOA, the average annual energy efficiency increases from 29.59% to 30.47%, an improvement of 3.0%.

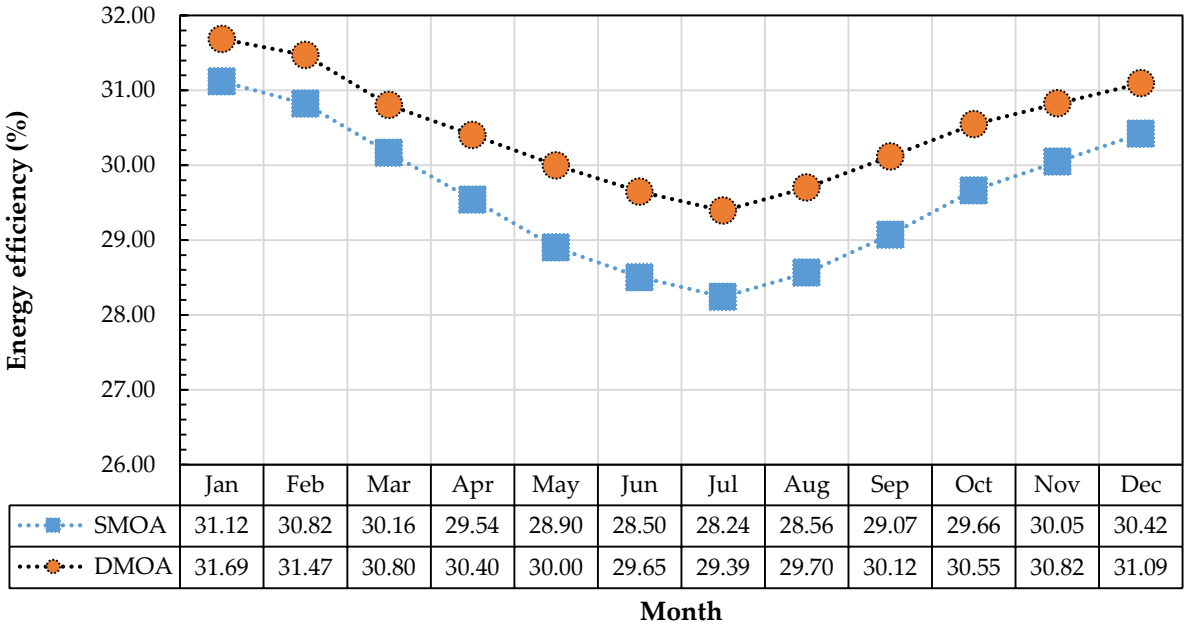

	Jan	Feb	Mar	Apr	May	Jun	Jul	Aug	Sep	Oct	Nov	Dec
SMOA	31.12	30.82	30.16	29.54	28.90	28.50	28.24	28.56	29.07	29.66	30.05	30.42
DMOA	31.69	31.47	30.80	30.40	30.00	29.65	29.39	29.70	30.12	30.55	30.82	31.09

Figure 5. Comparison of monthly energy efficiency with DMOA and SMOA.

3.3.4. Exergy efficiency

Figure 6 shows that, for both SMOA and DMOA, the monthly profile of exergy efficiency resembles that of energy efficiency. However, the values of exergy efficiency are generally lower than those of energy efficiency because there are several products in the form of heat and the exergy of a specific amount of heat is lower than its energy content. The enhancement in exergy efficiency due to the use of DMOA over SMOA increases as summer is approached. For example, in March, April, and May, SMOA gives an exergy efficiency of 18.35, 17.62, and 16.82%, while DMOA gives 19.14, 18.84, and 18.12%, implying increases of 4.3, 6.9, and 7.7%, respectively. On an annual basis, DMOA increases the exergy efficiency by 5.2% relative to SMOA.

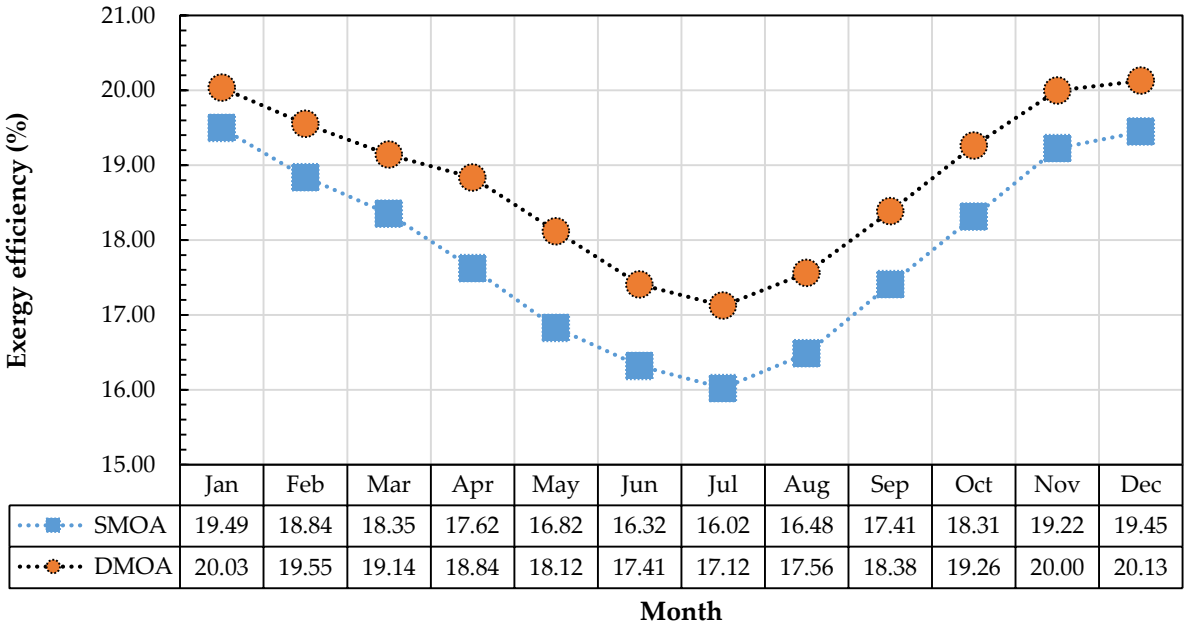

	Jan	Feb	Mar	Apr	May	Jun	Jul	Aug	Sep	Oct	Nov	Dec
SMOA	19.49	18.84	18.35	17.62	16.82	16.32	16.02	16.48	17.41	18.31	19.22	19.45
DMOA	20.03	19.55	19.14	18.84	18.12	17.41	17.12	17.56	18.38	19.26	20.00	20.13

Figure 6. Comparison of monthly exergy efficiency with DMOA and SMOA.

3.3.5. Useful electricity production

DMOA leads to a larger collector area, increasing useful electricity production. As Figure 7 shows, the difference in useful electricity production between the two optimization strategies starts at 61.7 kWh in January, and then rises to 182.2 and 491.9 kWh in March and May, respectively. During three summer months (July, August, and September), the difference in useful electricity production reaches 865.8, 863.0, and 810.9 kWh, respectively. This is beneficial as extra electricity produced during the summer months can help the power network cope with any unexpected deficits. In October, November, and December, DMOA gives 347.2, 193.8, and 101.7 kWh more electricity than SMOA. This indicates that a considerable improvement in electricity production can be achieved not only during the summer season, but for the whole year. In fact, throughout the entire year, SMOA gives 34577.0 kWh of electricity, but the corresponding value from DMOA is 39549.3 kWh, an improvement of 14.4%.

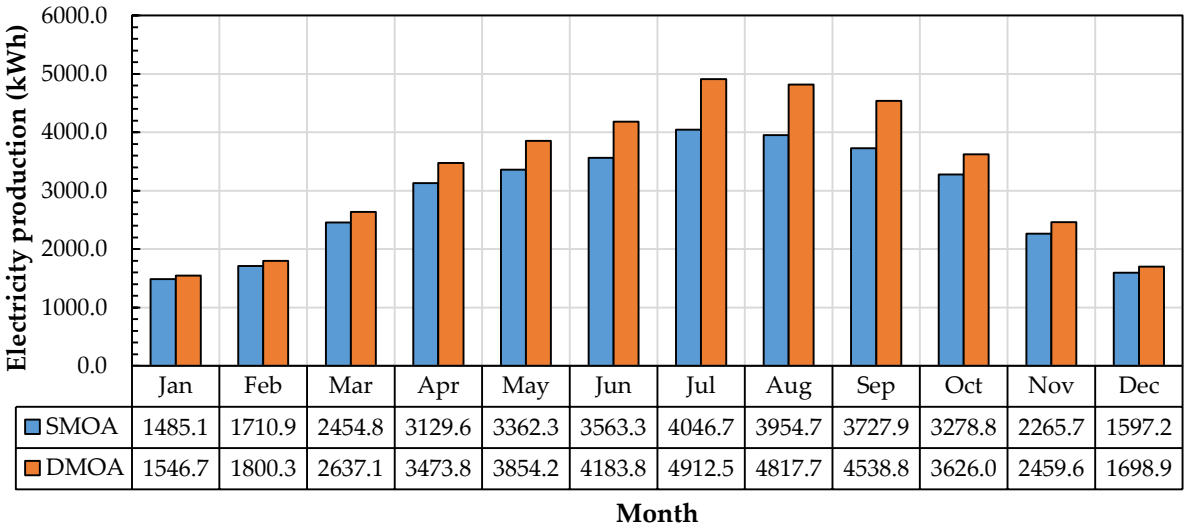

	Jan	Feb	Mar	Apr	May	Jun	Jul	Aug	Sep	Oct	Nov	Dec
SMOA	1485.1	1710.9	2454.8	3129.6	3362.3	3563.3	4046.7	3954.7	3727.9	3278.8	2265.7	1597.2
DMOA	1546.7	1800.3	2637.1	3473.8	3854.2	4183.8	4912.5	4817.7	4538.8	3626.0	2459.6	1698.9

Figure 7. Comparison of the monthly useful electricity production with DMOA and SMOA.

The power of a solar panel is the efficiency multiplied by the collected solar radiation over an area. When the solar radiation increases, the panel efficiency decreases. The positive influence of the increase in solar radiation can outweigh the negative influence of the drop in efficiency as a result of a hotter panel. This increases the electricity generated by the solar panels. The observed trend for power production rises during the hot seasons based on the above discussion, which is consistent with the literature, such as Ref. [30].

3.3.6. Useful heat production

The monthly profiles of useful heat production follow those of useful electricity production, as shown in Figure 8. With either optimization strategy, the values of useful heat production are significantly greater than those of useful electricity production. The lowest heat production is found for the coldest months of the year, i.e., January, February, November and December, in which 13069.4, 14859.9, 20322.6, and 14197.2 kWh of heat is produced with SMOA. With DMOA, however, those values increase by 7.1, 9.6, 9.5, and 8.3%, respectively. The largest increase occurs in the summer season, when the highest level of solar radiation is received. With

a heat production of 44438.1, 43580.2, and 41057.2 kWh, DMOA gives increases of 24.4, 22.8, and 19.8% in July, August, and September, respectively. On an annual basis, DMOA gives a heat production of 357757.0 kWh, which is a 16.1% improvement over SMOA.

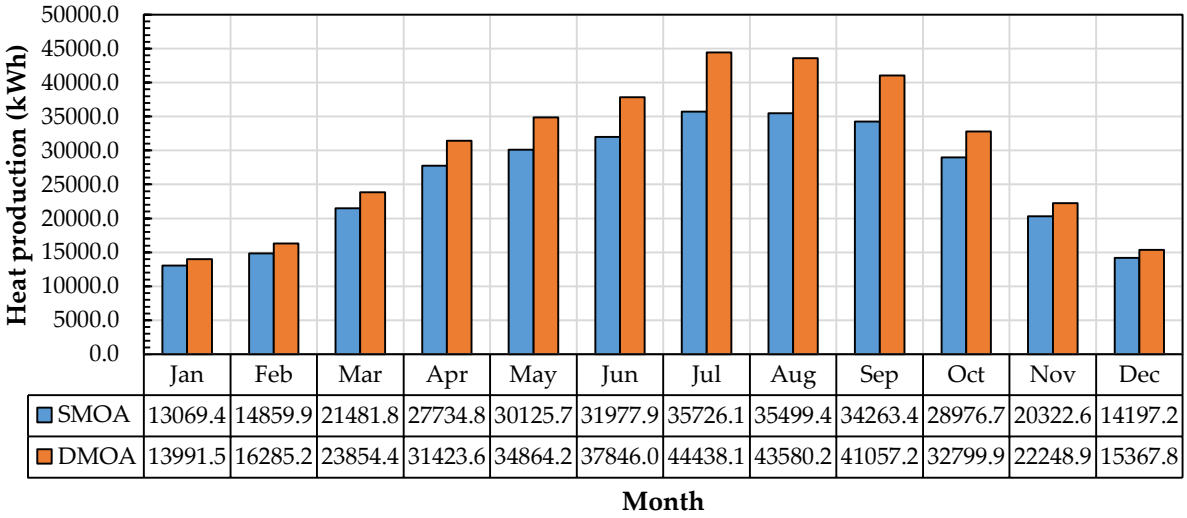

	Jan	Feb	Mar	Apr	May	Jun	Jul	Aug	Sep	Oct	Nov	Dec
SMOA	13069.4	14859.9	21481.8	27734.8	30125.7	31977.9	35726.1	35499.4	34263.4	28976.7	20322.6	14197.2
DMOA	13991.5	16285.2	23854.4	31423.6	34864.2	37846.0	44438.1	43580.2	41057.2	32799.9	22248.9	15367.8

Figure 8. Comparison of the monthly useful heat production with DMOA and SMOA.

3.3.7. Payback period

The payback period for SMOA is 5.56 years. When DMOA is applied, the collector area and, hence, the initial purchase price increases. Nonetheless, this is counterbalanced by improved generation capabilities and efficiencies, which tend to offset the higher upfront costs, reducing the payback period to 4.43 years for DMOA. This represents a 20.3% reduction relative to SMOA.

4. Conclusions

Rather than relying on conventional SMOA, this study uses DMOA, augmented with a combination of NSGA-II and TOPSIS, to optimize the performance of a solar-geothermal multi-generation system.

The results revealed that when compared with conventional SMOA, DMOA can improve the energy and exergy efficiencies, economic viability, and safety of a solar-geothermal multi-generation system. The annual production of electricity, heat, hydrogen, and water was found to increase by 14.4, 16.1, 13.5, and 14.3%, respectively. The average annual exergy and energy efficiencies were found to increase by 5.2 and 3.0%, respectively. Meanwhile, the payback period was found to decrease from 5.56 to 4.43 years, implying that DMOA is more economically competitive than SMOA. The hydrogen storage pressure was found to decrease by 4.4%, indicating improved safety with DMOA. Overall, this study demonstrates that the use of DMOA over SMOA can improve the exergy and energy efficiencies, economic viability, and safety of a solar-geothermal multi-generation system. This study opens several avenues for future work, including:

1. A feasibility study of the investigated system in different climatic regions,
2. Exploring the effects of price inflation or other economic indicators on the optimization results,
3. Adding an industrial plant to the multi-generation unit and investigating the hybrid system,
4. Evaluation of different storage technologies for the multi-generation unit.

References

[1] M. Temiz, I. Dincer, Concentrated solar driven thermochemical hydrogen production plant with thermal energy storage and geothermal systems, Energy. 219 (2021) 119554. https://doi.org/10.1016/J.ENERGY.2020.119554.

[2] U. Sajjad, N. Abbas, K. Hamid, S. Abbas, I. Hussain, S.M. Ammar, M. Sultan, H.M. Ali, M. Hussain, T. ur Rehman, C.C. Wang, A review of recent advances in indirect evaporative cooling technology, Int. Commun. Heat Mass Transf. 122 (2021) 105140. https://doi.org/10.1016/J.ICHEATMASSTRANSFER.2021.105140.

[3] A. Shahsavar, S. Entezari, I.B. Askari, H.M. Ali, The effect of using connecting holes on heat

transfer and entropy generation behaviors in a micro channels heat sink cooled with biological silver/water nanofluid, Int. Commun. Heat Mass Transf. 123 (2021) 104929. https://doi.org/10.1016/J.ICHEATMASSTRANSFER.2020.104929.

[4] F.A. Qureshi, N. Ahmad, H.M. Ali, Heat dissipation in bituminous asphalt catalyzed by different metallic oxide nanopowders, Constr. Build. Mater. 276 (2021) 122220. https://doi.org/10.1016/J.CONBUILDMAT.2020.122220.

[5] M. Saleem, K. Irshad, S.U. Rehman, M. Sufyan Javed, M.A. Hasan, H.M. Ali, A. Ali, M.Z. Malik, S. Islam, Characteristics and Photovoltaic Applications of Au-Doped ZnO–Sm Nanoparticle Films, Nanomater. 2021, Vol. 11, Page 702. 11 (2021) 702. https://doi.org/10.3390/NANO11030702.

[6] A.M. Abdelshafy, H. Hassan, J. Jurasz, Optimal design of a grid-connected desalination plant powered by renewable energy resources using a hybrid PSO–GWO approach, Energy Convers. Manag. 173 (2018) 331–347. https://doi.org/10.1016/J.ENCONMAN.2018.07.083.

[7] H. Sayyaadi, M. Saeedi Boroujeni, Conceptual design, process integration, and optimization of a solar CuCl thermochemical hydrogen production plant, Int. J. Hydrogen Energy. 42 (2017) 2771–2789. https://doi.org/10.1016/J.IJHYDENE.2016.12.034.

[8] A. Habibollahzade, E. Gholamian, P. Ahmadi, A. Behzadi, Multi-criteria optimization of an integrated energy system with thermoelectric generator, parabolic trough solar collector and electrolysis for hydrogen production, Int. J. Hydrogen Energy. 43 (2018) 14140–14157. https://doi.org/10.1016/J.IJHYDENE.2018.05.143.

[9] Y. Cao, H.A. Dhahad, A.G. ABo-Khalil, K. Sharma, A. Hussein Mohammed, A.E. Anqi, A.S. El-Shafay, Hydrogen production using solar energy and injection into a solid oxide fuel cell for CO2 emission reduction; Thermoeconomic assessment and tri-objective optimization, Sustain. Energy Technol. Assessments. 50 (2022) 101767. https://doi.org/10.1016/J.SETA.2021.101767.

[10] H.S.M. Yahya, T. Abbas, N.A.S. Amin, Optimization of hydrogen production via toluene steam reforming over Ni–Co supported modified-activated carbon using ANN coupled GA and RSM, Int. J. Hydrogen Energy. 46 (2021) 24632–24651. https://doi.org/10.1016/J.IJHYDENE.2020.05.033.

[11] F. Gutiérrez-Martín, L. Amodio, M. Pagano, Hydrogen production by water electrolysis and off-grid solar PV, Int. J. Hydrogen Energy. 46 (2021) 29038–29048. https://doi.org/10.1016/J.IJHYDENE.2020.09.098.

[12] A. Behzadi, A. Habibollahzade, P. Ahmadi, E. Gholamian, E. Houshfar, Multi-objective design optimization of a solar based system for electricity, cooling, and hydrogen production, Energy. 169 (2019) 696–709. https://doi.org/10.1016/J.ENERGY.2018.12.047.

[13] A.H. Keshavarzzadeh, P. Ahmadi, M.R. Safaei, Assessment and optimization of an integrated energy system with electrolysis and fuel cells for electricity, cooling and hydrogen production using various optimization techniques, Int. J. Hydrogen Energy. 44 (2019) 21379–21396. https://doi.org/10.1016/J.IJHYDENE.2019.06.127.

[14] R. Daneshpour, M. Mehrpooya, Design and optimization of a combined solar thermophotovoltaic power generation and solid oxide electrolyser for hydrogen production, Energy Convers. Manag. 176 (2018) 274–286. https://doi.org/10.1016/J.ENCONMAN.2018.09.033.

[15] M.S. Saleem, N. Abas, A.R. Kalair, S. Rauf, A. Haider, M.S. Tahir, M. Sagir, Design and optimization of hybrid solar-hydrogen generation system using TRNSYS, Int. J. Hydrogen Energy. 45 (2020) 15814–15830. https://doi.org/10.1016/J.IJHYDENE.2019.05.188.

[16] A. Izadi, P. Ahmadi, S. Bashiri Mousavi, I. Fakhari, A comparative optimization of a trigeneration

system with an innovative integration of solar Heliostat towers and Hydrogen production unit, Sustain. Energy Technol. Assessments. 47 (2021) 101522. https://doi.org/10.1016/J.SETA.2021.101522.

[17] H. Tebibel, Methodology for multi-objective optimization of wind turbine/battery/electrolyzer system for decentralized clean hydrogen production using an adapted power management strategy for low wind speed conditions, Energy Convers. Manag. 238 (2021) 114125. https://doi.org/10.1016/J.ENCONMAN.2021.114125.

[18] M. Koleva, O.J. Guerra, J. Eichman, B.M. Hodge, J. Kurtz, Optimal design of solar-driven electrolytic hydrogen production systems within electricity markets, J. Power Sources. 483 (2021) 229183. https://doi.org/10.1016/J.JPOWSOUR.2020.229183.

[19] S.M. Alirahmi, E. Assareh, N.N. Pourghassab, M. Delpisheh, L. Barelli, A. Baldinelli, Green hydrogen & electricity production via geothermal-driven multi-generation system: Thermodynamic modeling and optimization, Fuel. 308 (2022) 122049. https://doi.org/10.1016/J.FUEL.2021.122049.

[20] A. Farsi, I. Dincer, G.F. Naterer, Multi-objective optimization of an experimental integrated thermochemical cycle of hydrogen production with an artificial neural network, Int. J. Hydrogen Energy. 45 (2020) 24355–24369. https://doi.org/10.1016/J.IJHYDENE.2020.06.262.

[21] O. Siddiqui, I. Dincer, A new solar and geothermal based integrated ammonia fuel cell system for multigeneration, Int. J. Hydrogen Energy. 45 (2020) 34637–34653. https://doi.org/10.1016/J.IJHYDENE.2020.02.109.

[22] Y.E. Yuksel, M. Ozturk, I. Dincer, Development of a novel combined energy plant for multigeneration with hydrogen and ammonia production, Int. J. Hydrogen Energy. 46 (2021) 28980–28994. https://doi.org/10.1016/J.IJHYDENE.2020.12.113.

[23] H. Ishaq, I. Dincer, Dynamic modelling of a solar hydrogen system for power and ammonia production, Int. J. Hydrogen Energy. 46 (2021) 13985–14004. https://doi.org/10.1016/J.IJHYDENE.2021.01.201.

[24] M. Sangeetha, S. Manigandan, B. Ashok, K. Brindhadevi, A. Pugazhendhi, Experimental investigation of nanofluid based photovoltaic thermal (PV/T) system for superior electrical efficiency and hydrogen production, Fuel. 286 (2021) 119422. https://doi.org/10.1016/J.FUEL.2020.119422.

[25] S. Manigandan, V. Kumar, Comparative study to use nanofluid ZnO and CuO with phase change material in photovoltaic thermal system, Int. J. Energy Res. 43 (2019) 1882–1891. https://doi.org/10.1002/ER.4442.

[26] A. Sohani, A. Dehnavi, H. Sayyaadi, S. Hoseinzadeh, E. Goodarzi, D.A. Garcia, D. Groppi, The real-time dynamic multi-objective optimization of a building integrated photovoltaic thermal (BIPV/T) system enhanced by phase change materials, J. Energy Storage. 46 (2022) 103777. https://doi.org/10.1016/J.EST.2021.103777.

[27] A. Sohani, H. Sayyaadi, M. Azimi, Employing static and dynamic optimization approaches on a desiccant-enhanced indirect evaporative cooling system, Energy Convers. Manag. 199 (2019). https://doi.org/10.1016/j.enconman.2019.112017.

[28] El-Emam, Rami S., and Kamiel S. Gabriel. "Synergizing hydrogen and cement industries for Canada's climate plan–case study." *Energy Sources, Part A: Recovery, Utilization, and Environmental Effects* 43, no. 23 (2021): 3151-3165.

[29] Y. Noorollahi, H. Yousefi, R. Itoi, S. Ehara, Geothermal energy resources and development in Iran,

Renew. Sustain. Energy Rev. 13 (2009) 1127–1132. https://doi.org/10.1016/J.RSER.2008.05.004.

[30] A. Sohani, H. Sayyaadi, Providing an accurate method for obtaining the efficiency of a photovoltaic solar module, Renew. Energy. 156 (2020) 395–406. https://doi.org/10.1016/j.renene.2020.04.072.

[31] Kaya, Ibrahim, and Yasin Ust. "A new method to multi–objective optimization of shell and tube heat exchanger for waste heat recovery." *Energy Sources, Part A: Recovery, Utilization, and Environmental Effects* (2021): 1-18.

[32] A. Sohani, F. Delfani, A. Fassadi Chimeh, S. Hoseinzadeh, H. Panchal, A conceptual optimum design for a high-efficiency solar-assisted desalination system based on economic, exergy, energy, and environmental (4E) criteria, Sustain. Energy Technol. Assessments. 52 (2022) 102053. https://doi.org/10.1016/J.SETA.2022.102053.

Declaration of interests

☒ The authors declare that they have no known competing financial interests or personal relationships that could have appeared to influence the work reported in this paper.

☐The authors declare the following financial interests/personal relationships which may be considered as potential competing interests: